

The secret of immersion: actor driven camera movement generation for auto-cinematography

XINYI WU, Northwestern University, USA

HAOHONG WANG, TCL Research America, USA

AGGELOS K. KATSAGGELOS, Northwestern University, USA

Immersion plays a vital role when designing cinematic creations, yet the difficulty in immersive shooting prevents designers to create satisfactory outputs. In this work, we analyze the specific components that contribute to cinematographic immersion considering spatial, emotional, and aesthetic level, while these components are then combined into a high-level evaluation mechanism. Guided by such a immersion mechanism, we propose a GAN-based camera control system that is able to generate actor-driven camera movements in the 3D virtual environment to obtain immersive film sequences. The proposed encoder-decoder architecture in the generation flow transfers character motion into camera trajectory conditioned on an emotion factor. This ensures spatial and emotional immersion by performing actor-camera synchronization physically and psychologically. The emotional immersion is further strengthened by incorporating regularization that controls camera shakiness for expressing different mental statuses. To achieve aesthetic immersion, we make effort to improve aesthetic frame compositions by modifying the synthesized camera trajectory. Based on a self-supervised adjustor, the adjusted camera placements can project the character to the appropriate on-frame locations following aesthetic rules. The experimental results indicate that our proposed camera control system can efficiently offer immersive cinematic videos, both quantitatively and qualitatively, based on a fine-grained immersive shooting. Live examples are shown in the supplementary video.

CCS Concepts: • Computing methodologies → Procedural animation.

Additional Key Words and Phrases: automatic cinematography, camera movement generation, immersive film, actor-camera synchronization, director rule

ACM Reference Format:

Xinyi Wu, Haohong Wang, and Aggelos K. Katsaggelos. 2023. The secret of immersion: actor driven camera movement generation for auto-cinematography. *ACM Trans. Graph.* 1, 1 (March 2023), 18 pages. <https://doi.org/10.1145/nnnnnnnnnnnnnnnn>

1 INTRODUCTION

Immersion takes an essential place in designing art creations [Rose 2012]. Artists rack their brains to create an immersive environment in order to enhance the viewer experience and arouse resonance between actors and the audience. The appeal of artistic achievements

Authors' addresses: Xinyi Wu, Northwestern University, 633 Clark Street, Evanston, IL, 60208, USA, xinyi.wu2019.1@u.northwestern.edu; Haohong Wang, TCL Research America, San Jose, USA, haohong.wang@tcl.com; Aggelos K. Katsaggelos, Northwestern University, 633 Clark Street, Evanston, IL, USA, aggk@eecs.northwestern.edu.

Permission to make digital or hard copies of all or part of this work for personal or classroom use is granted without fee provided that copies are not made or distributed for profit or commercial advantage and that copies bear this notice and the full citation on the first page. Copyrights for components of this work owned by others than ACM must be honored. Abstracting with credit is permitted. To copy otherwise, or republish, to post on servers or to redistribute to lists, requires prior specific permission and/or a fee. Request permissions from permissions@acm.org.

© 2023 Association for Computing Machinery.

0730-0301/2023/3-ART \$15.00

<https://doi.org/10.1145/nnnnnnnnnnnnnnnn>

and business values leads to the pursuit of immersion in creative works for entertainment-related fields such as film production, game design, and virtual reality (VR).

Cinematography, as one of the techniques that provide 2D video-based artistic content for entertainment industries, has similarly faced the requirement to produce immersive outputs. Some directors conclude that the sense of immersion mainly arises from synchronization between camera and actor [Puschak 2017] so as to create illusions of reality. More specifically, such immersion can be subcategorized into spatial immersion, emotional immersion, and aesthetic immersion [Björk and Holopainen 2005; Mäcklin et al. 2019], emphasizing different aspects that strongly influence human perception. Camera movements such as tracking [Brown 2016] and shaking [Mekas 1962] are skills wildly utilized to immerse the audience spatially and emotionally by delivering visual responses of the actor's physical motions and psychological status, respectively. In terms of aesthetic immersion that can be controlled by camera, commonly it refers to composition-based aesthetics [Krages 2012], which can provide perceptual pleasure and attraction via carefully manipulated camera placements.

However, such a threshold of professional cinematographic skills results in difficulties for companies and individuals to yield expected high-quality immersive creations conveniently. To reduce costs and break knowledge barriers, the automatic generation process is then leveraged to mimic manual techniques for obtaining immersive film sequences. Traditional auto-cinematographic methods are based on merging multi-source short clips [Truong et al. 2016; Wang et al. 2019]. Lacking the controllability of cameras, the sense of immersion is coarsely handled by regularizing spatio-temporal [Arev et al. 2014] and semantic [Liang et al. 2012] consistency of the acting character in the resulting frames. With the focus switched to camera behavior planning [Subramonyam et al. 2018], camera angles and rails are pre-defined with encoded patterns to satisfy immersive shooting comprehensively [Galvane 2015] considering various cases. Yet suffering from the increasing customized scenarios, tremendous efforts can be taken to maintain and extend camera control patterns for enhancing immersion.

Learning-based approaches are then proposed to address such inflexibility. Partial answers target aesthetic immersion by using optimization [Yu et al. 2022a] or reinforcement learning [Yu et al. 2022b] to seek camera placements that maximize aesthetic composition efficiently. However, the outputted discrete placements fail to achieve spatial immersion, which requires a smooth and continuous track of the acting character. In another way, drone cinematography aims to estimate camera trajectories that can be consistent with physical motions of the actor by learning human motions and

optical flows from existing videos [Huang et al. 2021, 2019]. Despite manifesting advantages for spatial immersion to some degree, the long-distance drone shooting limits capturing the details of character status and simultaneously hampers handling emotional immersion. In order to obtain an enhanced immersive performance, methods [Jiang et al. 2021, 2020] synthesize camera behaviors based on high-level cinematic features extracted from footage of masterpiece. The fine-grain immersion is ensured by the introduced latent professional techniques when performing shooting. Yet, such methods are strongly dependent on the choice of the referred footage, and, the obtained immersive output is uncontrollable due to the implicitness in the latent space. That is to say, there is still lacking analysis of presenting immersion specifically and explicitly for the existing deep auto-cinematographic solutions.

In this paper we analyze the specifications including components of spatial, emotional, and aesthetic immersion that contribute to the overall sense of immersion in cinematography. These components are then combined into a high-level evaluation mechanism based on a fine-grained synchronization between actor and camera. Guided by such an immersion mechanism focusing on actor-camera consistency, we propose a deep camera control system in the 3D virtual environment that can synthesize actor-driven camera movements for obtaining high-quality immersive results.

The proposed system is structured with GAN framework. To satisfy spatial immersion, our camera is required to synchronize with the action performed by the character closely [Puschak 2017]. We design an encoder-decoder network as generator to synthesize camera trajectories by transferring human motion features. Differently from the coarse analysis in [Huang et al. 2021, 2019], we disarticulate actor poses into body regions that share homogeneous motions as the input of our encoder. In this way, the encoder is able to strengthen the learning of local movements when encoding kinematic latency and mimicking the hidden tracking decision of the director, which accordingly benefits the generation of immersive camera responses spatially.

We emphasize emotional immersion by creating camera shakiness [Morgan 2013] to express the mental status of the character during the decoding of camera rails. As the emotional prior, a compact factor is introduced in the latent representation densely, which describes the category and intensity of the psychological event. The decoder thus synthesizes additional shakiness upon the action-tracking behaviors corresponding to the given emotional factor. Simultaneously, a regularizer is incorporated to control whether the desired shakiness has been satisfied in the synthesized camera trajectory to further enhance the immersive performance emotionally.

In terms of aesthetic immersion, we focus on maintaining frame compositions that can attract human attention and increase viewer experience [Arnheim 1956] during the movements of our cameras. A self-supervised adjustor is utilized to modify the camera placement in the synthesized rail under the constraint of composition rules [Krages 2012; May 2020]. Unlike previous methods dealing with images [Hong et al. 2021; Li et al. 2018], our adjustment network manipulates the on-frame location of the foreground character based on the 3D-to-2D pose projection to derive an improved aesthetic layout.

Finally, the whole system achieves overall cinematographic immersion by producing cinematic sequences that can synchronize with the actor physically and psychologically following aesthetic composition. Such immersive shooting shows the ability to resemble the results of professional artists quantitatively and qualitatively, which experimentally validates the feasibility of the proposed immersion mechanism.

2 RELATED WORK

In this section, we review the progress made in research on auto-cinematography, specifically in terms of camera behavior planning and investigating the sense of immersion to improve the viewer experience.

2.1 Learning cinematographic camera control

2D video-based artistic content is an essential part of human entertainment, yet manual production of filmic videos is costly due to the high demand for labor and cinematic knowledge. As a result, there is growing interest in automatic cinematography. Broadly speaking, there are two main categories of methods for obtaining cinematic sequences automatically.

Editing-based approaches: A partial solution relies on editing the existing clips. For example, [Liang et al. 2012] created a scene dataset where each video clip was annotated with details such as time, place, and character. By parsing keywords in the given scripts, they were able to retrieve the best-matching clip for each scene and merge them into a complete cinematic video. However, as film is an art of consistency, gaps in story plots and visual perception must be avoided. To address this, [Arev et al. 2014] first estimate the salient object in the initial clip and then use a graph to optimize the spatio-temporal consistency of the labeled salient object during the retrieval of subsequent clips. [Wang et al. 2020] take this a step further by introducing the whole attention map of the video frame and simulating human gaze behavior to ensure consistent frame saliency. Instead, [Truong et al. 2016] focus more on the semantic consistency between the script description and video content. They achieve this by comparing the script text and the video annotation text using a term frequency-inverse document frequency (TF-IDF) similarity score [Manning 2009]. To strengthen this semantic constraint, [Wang et al. 2019] propose a multi-modal alignment strategy that regularizes the probability distribution between high-level semantic features extracted from the script texts and the retrieved video frames. In addition to considering the cross-modal semantic consistency between the script and video, [Yang et al. 2018] tackle the intra-clip and inter-clip semantic consistency by penalizing the temporal difference of the frame feature after dimensionality reduction. Overall, the editing-based approaches rely heavily on the diversity and quality of the footage database, which can result in limited flexibility when creating cinematic content and cause difficulties in practical usage.

Camera-based approaches: Another trend in methods imitates the workflow of directors. Instead of directly generating cinematic sequences, these methods first synthesize camera behaviors and then

use camera projection to create filmic videos. In the early stages of research, simple camera behaviors such as pan and tilt are pre-defined based on the script notation and controlled by speed in analytical ways to ensure that the focused character remains within the frame [Hayashi et al. 2014; Kim et al. 1998; Subramonyam et al. 2018]. To enhance the viewer experience, real-world director rules that control shot types and angles [Karakostas et al. 2020] are introduced as constraints in optimization methods for selecting satisfactory camera placements [Louarn et al. 2018; Yu et al. 2022a] or generating camera rails [Galvane 2015]. Furthermore, additional encoded rules for camera intrinsics such as focal length and focal distance [Bonatti et al. 2020; Pueyo et al. 2022] are utilized to optimize better shooting performance.

Recently, neural networks have shown their power in generation tasks. [Gschwindt et al. 2019] train a deep agent using reinforcement learning, which is capable of synthesizing camera trajectories based on the initial camera placement. To ensure high-quality shooting, they guide their training process with rewards derived from human preferences through real-time manual scoring for the shot. Taking a further step, [Yu et al. 2022b] construct reward functions based on two main aspects: aesthetics and fidelity. This allows regularization of director rules to consider not only aesthetic shooting, such as character visibility and consistency, but also to avoid possible occlusions and inappropriate shot angles that could hamper viewer observation.

However, the effort taken to encode camera patterns is endless. [Huang et al. 2019] proposes a novel way to transfer human motion behavior into camera trajectories. They design an encoder to extract human kinematics and optical flow based on the given human motion video. The motion features are then sent to a decoder network to generate camera-space movements. This method demonstrated a strong ability to automatically obtain high-quality tracking shots for moving humans. Building on this work, they design a style feature extractor [Huang et al. 2021] that can represent the shooting style of any filmic video as a low-dimensional vector. This vector can be combined with the observed human motions to determine the current camera shot. This approach simplifies the process of encoding camera patterns by leveraging human motion and filmic-style features to generate camera rails.

Yet, the focus of long-distance aerial shooting [Huang et al. 2021, 2019] lacks the fine-detailed camera control for meeting real-world cinematic requirements. To alleviate this problem, [Jiang et al. 2020] propose a cinematic feature space that can encode the shooting patterns of a real film clip and retarget them to a new 3D environment. This feature space is estimated by analyzing the inter-relationship of character poses in the frame, allowing for fine-grained analysis of camera behavior. In addition, they propose a key frame control strategy [Jiang et al. 2021] to provide more powerful stylistic constraints for the generated cinematic sequences. Overall, these works significantly improve the feasibility of camera-based auto-cinematography. However, few of them address the sense of immersion, which is a critical factor that greatly influences the quality of cinematic videos.

2.2 Investigating improved immersion

The sense of immersion was first highly concerned in the virtual reality (VR) field, where applications aim to create place illusions and plausibility [Skarbez et al. 2020] for immersing users through realistic visualizations [Chu et al. 2021], communications [Zhang et al. 2022], and telepresence [Arora et al. 2022]. Similarly, with the advent of new-generation visual devices, many works have been proposed to investigate and enhance the immersiveness of cinematic videos. These efforts include research on audio [Williams et al. 2022], visual [Leake et al. 2017], and haptic [Guillotel et al. 2016] signals. Given that over 80% of the brain's perceptions are visual, controlling camera behaviors has become one of the most critical factors in creating a sense of immersion in cinematic sequences.

Based on real-world experience [Flight 2021], the key factor in creating immersion is the ability to convey the actor's emotions to the audience using specific shooting techniques. [Kasahara et al. 2016] focus on addressing this cognitive response at the spatial level. Their findings show that when shots are offered from the same spatial direction as the actor, viewers report feeling more immersed in the environment they perceive. [Dang et al. 2020] further create consistent spatial camera movements learned from human motions to enhance the feeling of realism in outdoor shooting. Similarly, expressing the actor's emotions is also an essential part of immersion [Jones and Dawkins 2018; Visch et al. 2010]. The mental resonance between the actor and the audience strengthens the involvement in the scene. [Bonatti et al. 2021] learn a semantic space based on the crowd-sourced emotions from a large footage dataset. This semantic space is subsequently combined into the camera behavior generation to control the stylistic variance for expressing different emotions. In contrast, [Sayed et al. 2022] controls the appropriate steadiness of the camera for long-take shots. Some works also consider aesthetic frame compositions [AlZayer et al. 2021; Dang et al. 2022] to enhance immersive shooting performance by improving overall cinematic quality. However, to our knowledge, none of these works addresses cinematic immersion analytically or quantitatively. Additionally, there is still room for novel methods that enhance immersion by combining all of the main immersing factors.

3 METHOD

Our objective is to design a camera control system that can efficiently generate immersive cinematic video based on the 3D virtual environment for companies and individual artists.

To solve this problem, we analyze the real-world masterpiece and combine the specifications leading to the sense of immersion into a high-level evaluation mechanism. We then propose a GAN-based generation flow guided by such a mechanism, which is able to synthesize actor-driven camera movements automatically for obtaining cinematographic immersion. In the following section we will detail our methodology.

3.1 Specification analysis for filmic immersion mechanism

The pursuit of immersion is an everlasting topic for artistic creations. Followed by the evolution of visual devices in entertainment industry, cinematography has gained increasing popularity in film as well as other novel fields like virtual reality and game design

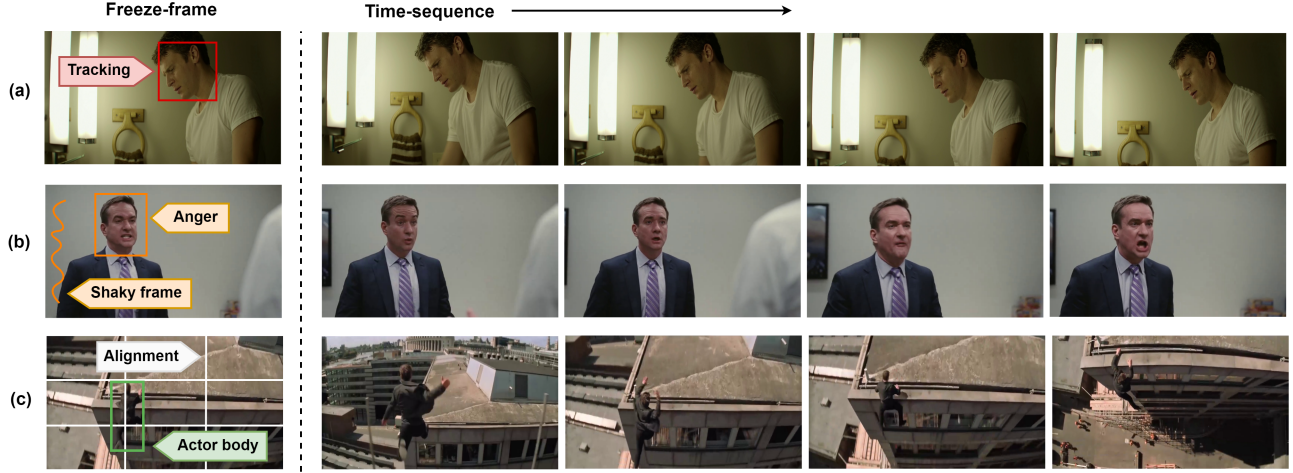


Fig. 1. Real-world cinematic examples (a), (b), and (c) demonstrate how spatial, emotional, and aesthetic immersion are achieved via shooting techniques using tracking camera, shaky camera and rule-of-thirds, respectively. Live clips are in the supplementary video.

[Rose 2012]. Meanwhile, market and audience call for high-quality immersive works that could leverage the advanced devices. Paying more attention to the sense of immersion in the production, creators need to think of two key questions (1) What can make the cinematic video immersive? and (2) How can we achieve it?

3.1.1 Empirical rules and techniques. In traditional cinematography, the mainstream interpretation considers that the sense of immersion comes from alive camera movements on behalf of the audience's eyes, which provides visual responses from a perspective of an invisible character staying inside the scenario [Flight 2021]. However, the perceptual engrossment of the audience is affected by multiple modalities. In [Björk and Holopainen 2005; Mäcklin et al. 2019], theoretically immersion can be subcategorized into the spatial, emotional and aesthetic level. Corresponding to such classification, practically directors create responses to capture not only the main actor's behavior but also its personality and involvement in the scene. These empirical rules for immersive camera control can be summarized as follows based on actor-camera synchronization [Puschak 2017]:

- Synchronize camera with actor's physical movements for spatial immersion
- Synchronize camera with actor's mental status for emotional immersion
- Synchronize camera with visual aesthetics existing between foreground actor and background for aesthetic immersion

Various shooting techniques are summarized based on audience feedback to implement the empirical rules above. As examples, orbit [Guzman 2021] and tracking [Brown 2016] camera are commonly utilized to follow the performed action feasibly for handling spatial immersion. When it comes to enhancing emotional immersion, visual responses can be intentionally created by zooming [Jacobs 2018] and shaky camera [Mekas 1962] as the expression of the actor's psychological status. In terms of visual aesthetics, a well-designed frame composition is considered beneficial to aesthetic immersion, where the camera should obey principles like eye-level framing

[Lannom 2019], 180-degree rule [Proferes 2005], or rule-of-thirds [Wright 2017]. Meanwhile, techniques targeting different types of immersion are leveraged in combinations to achieve the overall sense of immersion optimally.

3.1.2 High-level evaluation mechanism. Based on empirical rules and techniques, a high-level evaluation mechanism can thus be constructed by measuring actor-camera synchronization at spatial, emotional, and aesthetic level, in order to assess the immersive performance in the cinematic clip. Given a film sample V , we can obtain Z^h and Z^c to represent the behaviors of actor and camera in the scene, respectively. The score for spatial immersion I_s then can be defined as:

$$I_s = f_s(Z^h, Z^c), \quad (1)$$

where f_s denotes the operation to compare the feature-level consistency between actor and camera spatially based on the selected cinematographic technique.

Similarly, we can derive the score for emotional immersion by $I_e = f_e(Z^h, Z^c)$, while aesthetic immersion by $I_a = f_a(Z^h, Z^c)$. The measurement operations f_e and f_a vary according to the choices for techniques handling synchronizations related to emotion and aesthetics, respectively.

The quantified overall immersion I finally can be formed into a convex combination of the three subcategorized immersion scores as:

$$I = \alpha I_s + \beta I_e + (1 - \alpha - \beta) I_a, \quad (2)$$

Where α and β are both $\in [0, 1]$ and represent the weights controlling the trade-offs between different components due to stylistic variations among directors.

We leverage Equation (2) to guide the following camera movement generation. Due to the complexity of preferences toward different shooting techniques, in this paper, the design of f_s , f_e and f_a are followed by techniques of tracking camera, shaky camera, and rule-of-thirds in order to process the corresponding types of

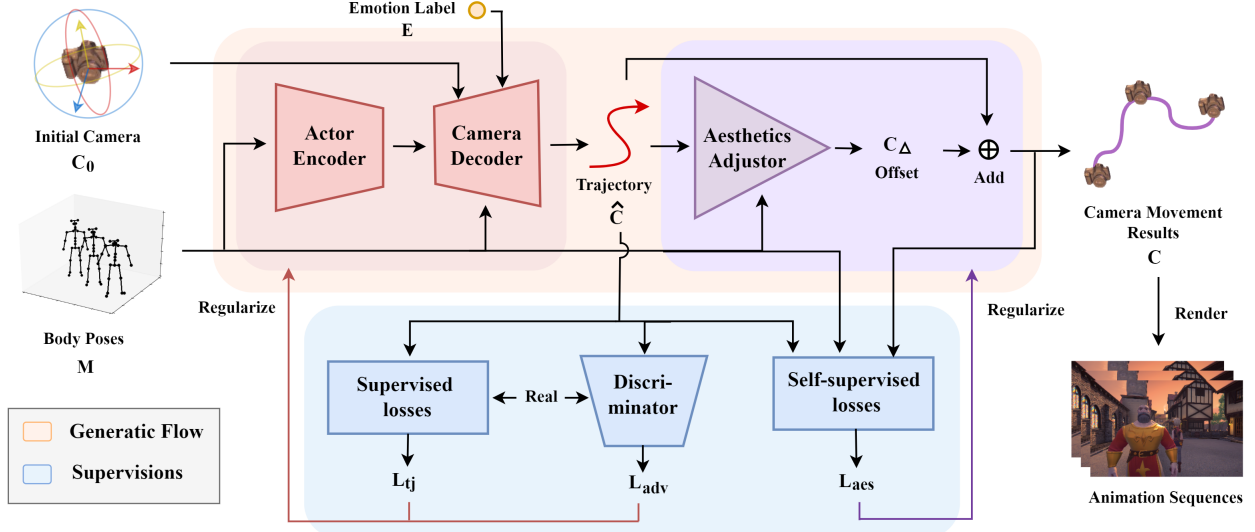


Fig. 2. The framework of our proposed immersive camera control system, which consists of two modules handling camera trajectory synthesis and visual aesthetics adjustment, respectively. The symbol \oplus represents the element-wise addition.

immersion. Note that the replacement of techniques will not affect the general framework regarding actor-camera synchronization. Details of the utilized three techniques can be seen in Appendix A.

As shown in Fig. 1, referring to footages in masterpieces, we expect that the synthesized actor-driven camera behaviors manage to track the performed action closely, create emotion-adapted camera shakiness, and maintain aesthetic composition under one-third alignment. Since Equation (2) is a heuristic strategy, it is verified via subjective experiments in Section 4. Simultaneously, its validity is also proven by showing the high-quality immersive performance of our generated cinematic sequences.

3.2 Framework of immersive camera control system

To automatically generate immersive camera movements, we propose a GAN-based framework for our camera control system in the 3D virtual environment. All the objects in the system share Q ($Q = 6$) degrees of freedom in position (x, y, z axis) and rotation (yaw, pitch, roll). Driven by actor behavior, we represent the movements of the focused character by a temporal set of T poses $M \in \mathbb{R}^{T \times JQ}$, where J is the number of joints in each pose. To depict the mental status of the actor, a non-negative emotion label E is utilized as the representation considering sentimental category and intensity compactly. Thus, given an initial camera placement $C_0 \in \mathbb{R}^Q$ decided by the user, our camera control system Υ can generate the following camera sequence $C \in \mathbb{R}^{T \times Q}$ as the result of immersive camera movement, forming

$$C = \Upsilon(M, E, C_0). \quad (3)$$

As shown in Fig. 2, in the generation flow an encoder-decoder based network G is designed to obtain the preliminary camera trajectory \hat{C} by transferring features learned from the information of actor behavior as:

$$\hat{C} = G(M, E, C_0). \quad (4)$$

Based on ground-truth samples created by professional artists, the hybrid trajectory loss \mathcal{L}_{tj} and adversarial loss \mathcal{L}_{adv} supervise our generated \hat{C} synchronizing with the actor's physical movements and psychological status, in order to satisfy spatial and emotional immersion.

However, due to the labor cost, the management is limited when it comes to manifesting perfect visual compositions in manually produced real samples. An additional adjustment network ψ is utilized to ensure aesthetic composition in each shot of \hat{C} for achieving aesthetic immersion thoroughly. Without using noisy labels, we conduct self-supervised learning based on the hybrid loss \mathcal{L}_{aes} , which regularizes visual aesthetics by analyzing the 2D projection of M . The offset C_Δ can then be obtained to modify camera placements in \hat{C} efficiently, avoiding over-adjusting or harming the existing performance of spatial and emotional immersion. Based on Equation (4), finally the resulting C is synthesized by:

$$C = \hat{C} \oplus C_\Delta = \hat{C} \oplus \psi(M, \hat{C}). \quad (5)$$

The details of camera trajectory synthesis are discussed in Section 3.3, while the process of visual aesthetics adjustment is shown in 3.4.

3.3 Camera trajectory synthesis

In order to generate a preliminary camera trajectory satisfying spatial and emotional immersion, we make efforts to train a neural network that is able to transfer features from actor space into cinematic space. The input actor feature X^h obtained from M, E , and C_0 is expressed as follow:

$$X^h = \{M, M^d, M^v, E, C_0^*\} \quad (6)$$

where

- M , M^d , and M^v are all $\in \mathbb{R}^{T \times JQ}$. M^d and M^v denotes the absolute difference and velocity, respectively, representing changes of joint-based spatial locations M between frame t and $t-1$. In order to align the temporal dimension with M , random noise is padded as the first-frame feature in M^d , and M^v .
- E is a constant $\in (0, E_{max}]$ while $E_{max} > 1$. Since cinematographic emotions can be classified into tense and relaxed ones [Wu et al. 2018], here $E < 1$ means the actor is performing a relaxed emotion and the smaller E the higher the relaxation. On the contrary, in the case of $E > 1$, the larger the higher the tension.
- $C_0^* \in \mathbb{R}^{T \times Q}$ denotes the features enhanced from initial camera placement C_0 by repeating it T times in the temporal domain.

Since the power of adversarial learning has been confirmed in generation-related work, we utilize GAN as our synthesis model to obtain the camera behavior $\hat{C} \in \mathbb{R}^{T \times Q}$ synchronizing with the actor physically and psychologically.

3.3.1 Network architecture. To make the transfer process more efficient, the generator G is designed with encoder-decoder architecture, where the intermediate latent representation is introduced to aid the transformation across different spaces.

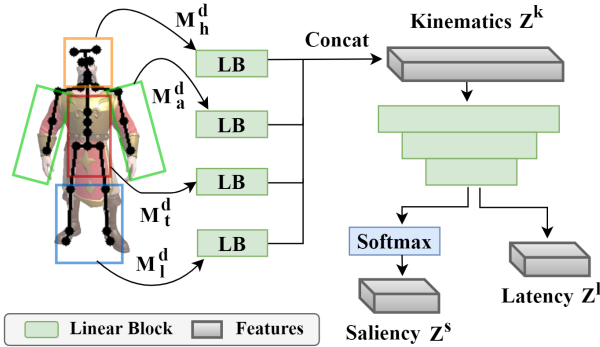


Fig. 3. The design of encoder in G . See text descriptions for details.

Actor encoder: During the encoding phase, we emphasize the learning of character movements to benefit spatial immersion in the result. To mimic director’s decision towards the focus among a range of concurring sub-motions, actor poses are disarticulated into 4 parts: head, arm, torso, and leg for a fine-grained strategy analysis. As shown in Fig 3, our encoder is fed with M^d , which is partitioned into M^d_h , M^d_a , M^d_t , and M^d_l to represent the corresponding body region, respectively. We apply a set of linear blocks consisting of a dense layer, a layer normalization, and a leaky ReLu to extract local motion features in different body regions. These region-wised features are then concatenated together to form the overall kinematic embeddings Z^k . After feature compression by several linear blocks, apart from obtaining the latent feature Z^l , based on a softmax operator we are also able to derive a saliency map Z^s that intuitively

learns the hidden tracking strategy.

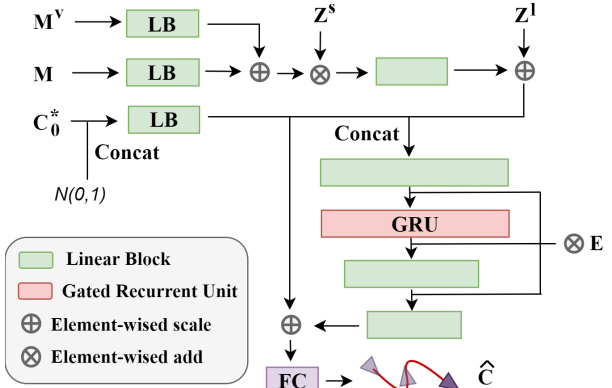


Fig. 4. The design of decoder in G . See text descriptions for details.

Camera decoder: We decode Z^l from the latent space to the expected cinematic space with the further introduced features extracted from M^v , M and C_0^* . To enrich the limited information, C_0^* is concatenated with random noise for obtaining features, which can simultaneously benefit the robustness of the generation process. Taking advantage of the saliency map Z^s outputted from the encoder, features representing the tracking strategy for spatial immersion are multiplied with the fused human motion features and subsequently combined into the latent representation by adding to Z^l . During the decoding phase, besides linear blocks, we leverage Gated Recurrent Units (GRUs) [Chung et al. 2014], which is an efficient variant of RNN confirmed to outperform LSTM structure for handling sequential data. Meanwhile, we densely incorporate the emotion factor E into the decoding process multiple times in order to guide the enhanced cinematic expression for emotional immersion. In order to focus on learning the temporal differences of the camera location sequence, features from C_0^* are not only combined to the latent space but also contribute to the output \hat{C} by applying a skip connection at the end of the decoder.

Discriminator: The architecture of our discriminator follows the design of Siamese network [Chopra et al. 2005], which is widely utilized for distinguishing image-based [Taigman et al. 2014] and sequence-based [Lee et al. 2019] data. Given a pair of real and generated fake samples denoted as \hat{C}' and \hat{C} , respectively, we make use of two identical shared-weight branches, where each of them consists of three layers of linear blocks, to extract features for cinematic dynamics in both samples. The real and fake features are then fused and sent to the following classifier to determine the similarity between \hat{C}' and \hat{C} , reflecting the generation performance adversarially.

3.3.2 Loss functions. The training of G is supervised by adversarial loss \mathcal{L}_{adv} and trajectory loss \mathcal{L}_{tj} , where \mathcal{L}_{tj} is hybridized with components regularizing the synthesized trajectory in terms of point level, feature level, and shakiness level compared with the real

professional samples.

Point loss: \mathcal{L}_{mse} is constructed by calculating an enhanced L2 distance between ground-truth \hat{C}' and generated \hat{C} considering total variation [Mahendran and Vedaldi 2015] for temporal smoothness:

$$\mathcal{L}_{mse} = \|\hat{C}' - \hat{C}\|_2^2 + \sum_{t=1}^{T-2} (\hat{C}_{t+1} - \hat{C}_t) + (\hat{C}_t - \hat{C}_{t-1}), \quad (7)$$

Where T denotes the total number of frame time t ranging from 0 to $T - 1$.

Feature loss: Since VGG [Simonyan and Zisserman 2014] has been widely used to extract effective features consistent with human perception, here we make use of it to regularize our generated camera trajectories close to the real samples in the feature space, as:

$$\mathcal{L}_{feat} = \|VGG(\hat{C}') - VGG(\hat{C})\|_2^2. \quad (8)$$

Shakiness loss: We attempt to align the camera shakiness in the generated trajectory with that shown in the well-designed real sample. By constraining the required visual unsteadiness, accordingly the emotional immersion can be improved in the results. Since shakiness arises from frequent changes of direction during the camera movement, we design an algorithm f_{shake} to measure the shaky performance of a camera sequence based on analyzing the amplitude and frequency of the shake.

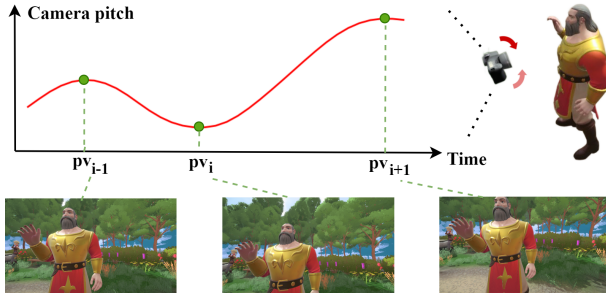


Fig. 5. An example of shaky camera functioning in the pitch axis. We zoom in the trajectory to demonstrate the occurrence of visual unsteadiness.

As shown in Fig. 5, when camera movements occur on a specific axis, we collect time points where the velocity of camera equals zero to represent directional changes for shakiness, which is denoted as $Pv = \{pv_0, pv_1, \dots, pv_N\}$. The corresponding shaky performance along this axis can then be measured as a constant by:

$$f_{shake}(\tilde{C}^q) = \sum_{i=1}^N \frac{|\tilde{C}_{pv_i}^q - \tilde{C}_{pv_{i-1}}^q|}{pv_i - pv_{i-1}}, \quad (9)$$

Where q denotes a certain axis among Q degrees of freedom of an arbitrary camera sequence \tilde{C} and i iterates elements in Pv . The overall trajectory shakiness $\tilde{C}_{sk} \in \mathbb{R}^Q$ is obtained by performing f_{shake} on each camera movement axis.

Thus, the camera shakiness in our generated trajectory can be weakly supervised by

$$\mathcal{L}_{sk} = \|\hat{C}'_{sk} - \hat{C}_{sk}\|. \quad (10)$$

Adversarial loss: Taking the advantage of the GAN framework, our discriminator D tries its best to distinguish between real and fake pairs through maximizing the loss

$$\mathcal{L}_{adv}^d = \mathbb{E}[\log D(\hat{C}', \hat{C}')] + \mathbb{E}[\log(1 - D(\hat{C}', \hat{C}))]. \quad (11)$$

Based on the adversarial training, our generator G is forced to improve the synthesized results in order to fool D by minimizing the function:

$$\mathcal{L}_{adv}^g = \mathbb{E}[-\log(D(\hat{C}', \hat{C}))]. \quad (12)$$

In summary, combining all the regularizers above, the final loss function for the generator G can be formulated as

$$\mathcal{L}_g = \lambda_{mse} \mathcal{L}_{mse} + \lambda_{feat} \mathcal{L}_{feat} + \lambda_{sk} \mathcal{L}_{sk} + \lambda_{adv} \mathcal{L}_{adv}^g. \quad (13)$$

3.4 Visual aesthetics adjustment

3.4.1 Short-cut for fast adjustment. As we mentioned before, the noisy composition-related labeling hampers the correct guidance for G to generate results with satisfactory aesthetic immersion. Referring to Equation (5), in order to enhance aesthetic compositions in \hat{C} , we design network ψ to suggest adjustment based on analyzing the on-frame location of the actor in a self-supervised way. Benefiting from progress in G , it can be assumed that the actor is located **stably** on each shot of \hat{C} due to the achieved spatial synchronization. Thus, instead of modifying placements in the whole camera sequence, ψ can focus on ensuring visual aesthetics for the first frame, which reforms Equation (5) as:

$$C = \hat{C} \oplus \psi(M_0, \hat{C}_0) = \hat{C} \oplus C_{0\Delta}, \quad (14)$$

where $\hat{C}_0 \in \mathbb{R}^Q$ and $M_0 \in \mathbb{R}^{JQ}$ represent the first-frame camera placement and actor pose, respectively, in order to learn an adaptive strategy for adjustment. The obtained first-frame offset $C_{0\Delta} \in \mathbb{R}^Q$ is applied onto each frame of \hat{C} . In this way, we not only control compositions for aesthetic immersion, but also preserve the generated dynamics for spatial and emotional immersion when finally outputting C .

3.4.2 Constraints for aesthetic composition. We follow rule-of-thirds [Krages 2012] to constrain the expected compositions that favor aesthetic immersion. Based on our environment, the utilized rules are summarized into a decision tree to guide the adjustment.

As shown in Fig. 6, frames are gridded with 4 lines to represent one-third alignment. We consider factors of actor pose and shot side (i.e. from which side the actor is shot) to determine which one or two specific lines should be counted for aesthetic composition. Instead of understanding image pixels like [Hong et al. 2021; Li et al. 2018], we project the 3D pose onto the corresponding 2D shot so as to judge whether the actor is aesthetically placed. As a simplification, we locate the actor using the body center, which is the weighted mean joint projected on the frame. The aesthetics problem can then be transformed into a distance problem between the body center and candidates of alignment lines, rather than digging into image features.

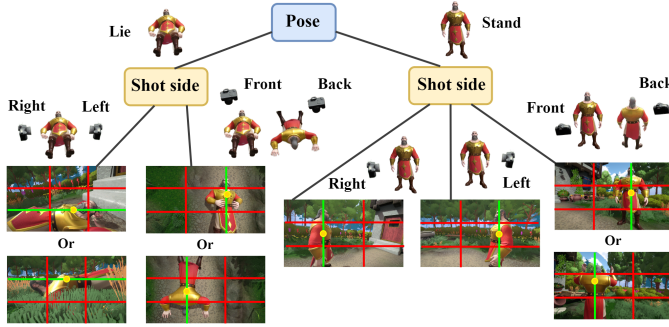


Fig. 6. Details of the summarized decision tree. Based on different cases, the on-frame body center (labeled as yellow dot) should stay on the specific alignment line (labeled in green) to achieve visual aesthetics.

3.4.3 Network and self-supervised losses. To cooperate with the projection-based composition strategy, network ϕ is designed for understanding the process of camera projection. As shown in Fig. 7, fed with M_0 and \hat{C}_0 , the whole architecture leverages attention blocks [Vaswani et al. 2017] to estimate the adjustment $C_{0\Delta}$. With the aid of transformation that combines the hidden self-attention Z^ω with the latent projection feature Z^γ , we expect only the on-frame joints, which highly influence the aesthetic composition, are emphasized via attention during learning.

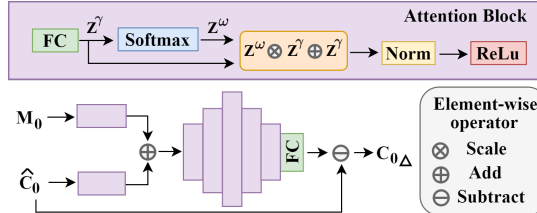


Fig. 7. The architecture of adjustment network ϕ .

The training of ϕ is self-supervised by a hybrid loss function \mathcal{L}_{aes} that handles not only the regularization of visual aesthetics but also the principle of proximity for the adjustment.

Composition loss: Given M_0 and the adjusted placement $\hat{C}_0 + C_{0\Delta}$, we can obtain the projected 2D actor pose $M_{2d} \in \mathbb{R}^{J \times 2}$ using camera projection and derive candidates of alignment $A_l \in \mathbb{R}^{2 \times 2}$ following decision tree shown in Fig. 6 (see Appendix B for details). The on-frame body center can then be located by calculating the weighted mean joint of M_{2d} , which is denoted as $\bar{M}_{2d} \in \mathbb{R}^2$. We thus can constrain aesthetic frame composition by regularizing the minimum distance between \bar{M}_{2d} and A_l as:

$$\mathcal{L}_{cmp} = \min(||\bar{M}_{2d} - A_l^0||_2, ||\bar{M}_{2d} - A_l^1||_2), \quad (15)$$

where A_l^0 and A_l^1 represent the two candidate alignments that are both $\in \mathbb{R}^2$. In the case there is only one alignment line determined by the decision tree, A_l^0 and A_l^1 are set equal.

Adjustment loss: In order not to over-adjust the original \hat{C}_0 , we design a constraint based on the estimated $C_{0\Delta}$ as:

$$\mathcal{L}_{adj} = ||C_{0\Delta}||_2, \quad (16)$$

Visualization loss: Due to the respect of user preference, we expect to preserve the original visualization of the actor presented by \hat{C}_0 , which can also be referred to shot type (e.g. full, medium, close shot) that strongly affects human perception. Thus, a contrastive regularizer is created to monitor the consistency of the on-frame and off-frame joints before and after adding the offset $C_{0\Delta}$ as:

$$\mathcal{L}_{vis} = M'_b \cdot (1 - M_b) + (1 - M'_b) \cdot M_b \quad (17)$$

where \cdot represents dot product. M'_b and M_b are both $\in \mathbb{R}^J$ obtained by binarizing the corresponding 2D pose projection (see Appendix B) via $\hat{C}_0 + C_{0\Delta}$, respectively.

In summary, the hybrid aesthetic loss function \mathcal{L}_{aes} that supervises the training of adjustment network ϕ can be formed into:

$$\mathcal{L}_{aes} = \lambda_{cmp} \mathcal{L}_{cmp} + \lambda_{adj} \mathcal{L}_{adj} + \lambda_{vis} \mathcal{L}_{vis}. \quad (18)$$

4 EXPERIMENTS AND RESULTS

In this section, we specify the experimental details for training the system and demonstrate the effectiveness of various components in our framework through an ablation study. The sense of immersion in our cinematic results is evaluated following the proposed mechanism in terms of spatial, emotional, and aesthetic level, compared to other feasible models. Please refer to the supplementary video as a complement for the qualitative evaluation.

4.1 User interface

An Unity3D application is created to provide a 3D virtual environment with several user interfaces for mimicking real-world cinematography. Different settings of cinematic resources (e.g. stage, character, action) can be selected when designing customized creations. In addition, users are able to edit camera behaviors through timelines and monitor the shooting based on the camera panel as well as real-time camera view. The designed camera placements or trajectories can be exported for research analysis. For practical usage, our model is also deployed as a plugin in the environment so as to benefit cinematic production in an immersive way.

4.2 Dataset

Samples for trajectory generator G : As we presented before, G generates camera trajectories based on the performed movement and emotion of the actor. Our environment provides a rich database of 590 character actions with additional 15 types of emotional descriptions. Each text-based emotion is mapped into a 5-scale emotion factor $\in \{0.5, 0.75, 1, 1.5, 2\}$ referring to its semantic category and intensity, which denotes *relax-more*, *relax-less*, *neutral*, *tense-less*, *tense-more* from small to large.

Under different combinations of physical and psychological status, we ask professional artists to manually shoot the actor by simulating immersive masterpieces (e.g. *Mindhunter*, *Succession*) with the use of specific cinematographic techniques (i.e. tracking camera,



Fig. 8. Functional zones of our user interface. Zone 1 works for the overall scene view and animation display. Zone 2 visualizes the camera view. In Zone 3, users are able to edit camera and actor behaviors via dragging and dropping blocks on the timeline, where detailed management can be processed with pop-up menus Zone 4 and 5, respectively.

shaky camera, and rule-of-thirds). These camera movement samples are exported via the user interface, which takes 20% of our dataset. Following the manual samples, the left 80% of the dataset is synthesized based on the symmetry among the actions and enhancement of the camera shakiness in order to fit the required emotion factor. We finally obtain 25,230 sliced samples totaling 1,135,350 frames to train our GAN network. In the test phase, 5550 unsliced samples are randomly picked to mimic the real user testing to evaluate the performance.

Samples for aesthetics adjustor ϕ : Since the whole training process for ϕ is self-supervised, we only need to prepare the input initial camera placement with the corresponding actor pose for analyzing camera projection. The camera placement is generally 100% synthesized except few percent of frequently-used locations collected from professional artists. To include enough spots where practically the user might choose to place the camera, extending the design in [Yu et al. 2022a], we generate several sphere meshes centered by the actor with multiple distances of radius and obtain 481,536 possible placements by collecting mesh points. Simultaneously, we retrieve 57 types of initial poses based on the action database as the possible pose input. Given combinations of different camera placements and actor poses, we remove the pair that derives the blank shot after projection and obtain 13,066,689 samples for our final dataset. 80% of them are separated randomly for training purpose while 20% are used for testing.

4.3 Implementation details

All the networks and losses are implemented in Pytorch. Some of our loss functions are mathematically smoothed in order to achieve differentiability in practice. We first pretrain our generator G with 100 epochs using only \mathcal{L}_{mse} . The Adam optimizer [Kingma and Ba 2014] is utilized with batch size of 10. The initial learning rate is set to 0.005 and gets decreased every 25 epochs divided by 10. Following the same optimizer and batch size, G and D are then trained adversarially with 45 epochs, where both the learning rates are set to 0.0001. Loss components for G are weighted as follows: $\lambda_{mse}=10$, $\lambda_{feat}=0.5$, $\lambda_{sk}=1$, $\lambda_{adv}=0.2$. In terms of ϕ , the convergence is achieved based on 35 epochs' of training with the batch size of

1024 and Adam optimizer. The learning rate is initialized with 0.002 and decreased 10 times each 10 epochs. We set the weights for loss components in \mathcal{L}_{aes} as: $\lambda_{cmp}=1$, $\lambda_{adj}=0.25$, $\lambda_{vis}=0.01$.

4.4 Ablation study

4.4.1 Evaluation of camera trajectory generation. We evaluate the effectiveness of our trajectory generator G by assessing the quality of the generated camera trajectory. In the evaluation, G is compared with the other three variants using metrics: MSE, LPIPS [Simonyan and Zisserman 2014], FID [Heusel et al. 2017] and cosine distance of trajectory shakiness (i.e. CosD_{sk}) on the testing dataset. As shown in Table 1, the pretraining model performs the best on MSE, but loses distinctly on the other feature-based metrics. On the contrary, the aid of adversarial training as well as the cooperation of \mathcal{L}_{feat} increase the similarity in the feature domain between real and fake samples stably (see results of G w/o \mathcal{L}_{sk}). We further calculate CosD_{sk} to visualize the performance of the learned camera shakiness C_{sk} (please refer to Equation (9)) via comparing with that of real one. It is obvious that by introducing \mathcal{L}_{sk} , our final G model largely outperformed others in terms of controlling camera shakiness. In a nutshell, we can conclude our final G model achieves a good trading-off between all the shown metrics.

Table 1. Comparison between G and its variants following different training strategies. All the metrics are the lower the better. The best results are labeled bold while second best in italic.

Model Name	MSE	LPIPS	FID	CosD_{sk}
Pretrain	0.0082	0.0510	0.0702	0.2935
G w/o \mathcal{L}_{feat} & \mathcal{L}_{sk}	0.0149	0.0477	0.0739	0.2569
G w/o \mathcal{L}_{sk}	0.0135	0.0385	<i>0.0681</i>	0.2509
G	0.0124	0.0405	0.0634	0.2380

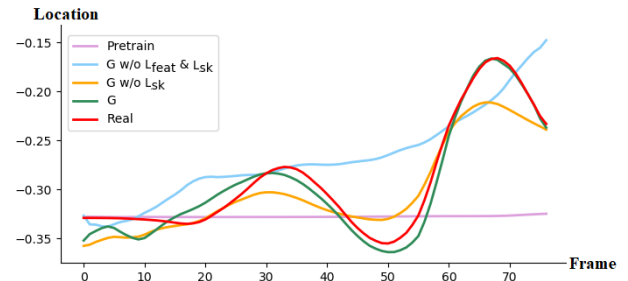


Fig. 9. An qualitative example visualizing the quality of generated camera trajectories, where we demonstrate camera location on a certain axis over the temporal evolution.

Meanwhile, the qualitative example Fig. 9 also manifests the same conclusions we draw from the table analysis. When \mathcal{L}_{mse} dominates the training, the generated trajectory can be over-smoothed, even remains to be still for some exciting scenarios (e.g. shooting intense actions or emotions). In avoid of losing fine-details for depicting motion trend, with the hybrid loss, our final G model can capture high-level features and force the generation to fit the shape of the real trajectory sample.

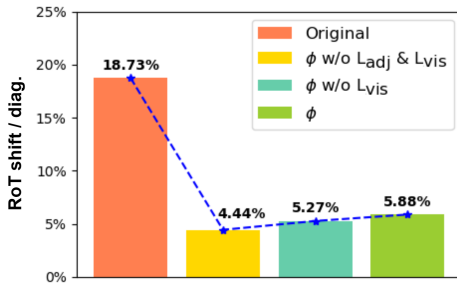


Fig. 10. The enhancement of aesthetic composition following rule-of-thirds based on adjustments from ϕ and its variants.

4.4.2 Evaluation of visual aesthetics adjustment. The performances of adjustment models under different training strategies are demonstrated in Fig. 10. We calculate rule-of-thirds (RoT) shift, which is the minimum distance between the on-frame body center \bar{M}_{2d} and candidates of alignment A_l (see Equation (15)), normalized by the diagonal of the shot. It is obvious that, by applying adjustment, the average shift is decreased distinctly from around 18% of the shot diagonal to around 5%. On the other hand, the average RoT shift between ϕ and its variants is subtle, which differs by less than 15 pixels for a shot of 1080P.

Table 2. Comparison of practical factors that influence the assessment of adjustment.

Model Name	RoT Increase \uparrow	Adjusted Distance \downarrow	Visibility Accuracy \uparrow
ϕ w/o \mathcal{L}_{adj} & \mathcal{L}_{vis}	73.25%	0.7860	46.11%
ϕ w/o \mathcal{L}_{vis}	70.54%	0.1191	47.87%
ϕ	66.54%	0.1473	71.08%

We also test other factors that highly influence human perception for assessing suitable adjustment in practice. In Table 2, RoT increase represents the aesthetic improvement compared to the original frame composition. The adjusted distance is calculated by MAE between the camera placement before and after adjustment. In terms of visibility accuracy, we compute how many percentages of body joint are correctly visualized on the frame. It can be seen that, though similar performance shown in RoT increase, there is a huge difference between results for adjusted distance and visibility accuracy. Overall speaking, our final ϕ earns the best trading-off in comparison with other variants. Fig. 11 illustrates an example comparing the results of adjustment qualitatively. We can observe that our final ϕ model can provide the enhanced aesthetic composition by suggesting an adjustment that is proximate to the original settings.

4.5 Quantitative evaluation of immersion

To quantitatively assess the sense of immersion in results generated from the overall system Υ , we follow the strategy of our proposed evaluation mechanism (see Section 3.1.2). Based on Equation (2), different weightings for α and β are considered in the evaluation.

4.5.1 Spatial immersion. When α is set 1 and β is set 0 in Equation (2), the evaluation tends to focus on spatial immersion, assessing the actor-camera synchronization at the spatial level. We compare our method with two other camera controllers. One is an optimization model [Yu et al. 2022a]. Considering the on-frame fidelity and aesthetics of a moving actor, [Yu et al. 2022a] can output well-designed camera sequences where each placement is selected from a pre-defined camera set scattered around the actor. The other one is the general tracking method, which virtually ties a camera C_0 to the head or pelvis of the actor for handling close shots or medium-to-full shots, respectively. Such a method can easily follow the movement of an actor at a low cost and is widely used in game design [Burelli 2016] and video production [Brown 2016].

For evaluating the spatial immersion, the three methods are tested based on the 3D virtual environment, where we randomly pick 37 untrained action samples with $T = 45$ frames to depict the movement of the character M . In the testing, the initial camera placement C_0 is given by the first-frame result of optimization model [Yu et al. 2022a], while the emotion label E is set to 1. We extract the mean velocity of the action as the spatial actor feature Z_s^h . Similarly, for each method, the spatial camera feature Z_s^c is represented by camera velocity between frames. All the obtained features are $\in \mathbb{R}^{(T-1) \times Q}$ and normalized to $[0,1]$. We introduce Hausdorff Distance (HD) as the metric to measure how Z_s^h is synchronized with Z_s^c .

In the left of Fig. 12, the result of HD shows that our system outperforms the other two models in terms of shooting in a way that is consistent with the physical behavior of the actor. The optimization model [Yu et al. 2022a] tends to avoid switching cameras when the actor is performing an action. Thus most of the generated camera behaviors of [Yu et al. 2022a] here remain to be static, having difficulty following character movement. When it comes to the general tracking method, it can partially synchronize with the actor. However, such synchronization is limited due to focusing only on the head or pelvis motion. Compared to other camera controllers, our system is able to preserve the overall trend of character movement stably, which can be seen in the right part of Fig. 12. We can also observe that the Z_s^c obtained from our model is not exactly as same as Z_s^h . This is because our model manages to mimic human decisions in cinematography, learning an appropriate saliency distribution for each body part to achieve better spatial immersion.

4.5.2 Emotional immersion. When we set α to 0 and β to 1 for Equation (2), the evaluation framework assesses emotional immersion, which expects the camera controller to create suitable shooting responses synchronized with the psychological presentation of the actor. Since currently there are few works addressing this problem in the film auto-cinematography area, here we simulate comparable models by removing the emotional enhancement factors in our method. The emotion-related variances in the dataset are taken out during training so as to imitate the performance of a plain camera that is mostly insensitive to the given mental status of the actor. Based on the original training dataset, with the disabled \mathcal{L}_{sk} we can also obtain a weak emotional camera for comparison.

All the methods are tested with the same samples used for evaluating spatial immersion. In order to observe changes in camera



Fig. 11. A qualitative example comparing the aesthetic adjustment of different models. The candidates of alignment A_l are labeled in green while the orange dot represents the on-frame body center \bar{M}_{2d} .

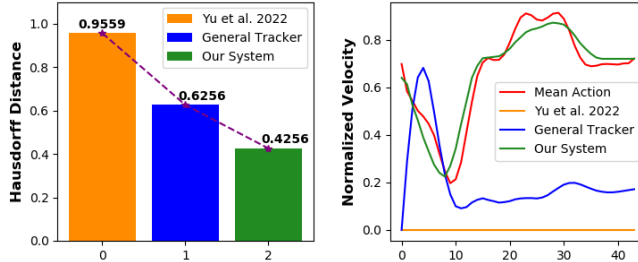


Fig. 12. Comparison of performance on spatial immersion. Left: results of HD, the lower the better. Right: an exampled visualization of spatial-level synchronization between Z_s^h (in red) and Z_s^c from different camera controller models based on a certain degree of freedom.

Table 3. Comparison of emotional immersion over the correlation between character emotion and camera shakiness.

Model Name	PCC \uparrow	SRCC \uparrow	KRCC \uparrow
PlainCam	0.7748	0.7822	0.7607
EmoCam	0.8017	0.8112	0.7652
Our System Υ	0.9235	0.9356	0.9153

behaviors adapted to the expressed emotion, based on each combination of M and C_0 , models are run N times using a list of N different E s. Such E list can be leveraged to represent the emotional actor feature $Z_e^h \in \mathbb{R}^N$, describing its mental evolution in the scenario. Correspondingly, for each run of a model, we collect the trajectory shakiness per degrees of freedom (DoF) of the camera result to form the representation of the emotional camera feature $Z_e^c \in \mathbb{R}^N$. Then, the actor-camera synchronization in terms of the emotional level can be evaluated by the correlation between Z_e^h and Z_e^c .

As shown in Table 3, we calculate 3 types of correlation coefficients, including Pearson (PCC), Spearman Rank (SRCC), and Kendall Rank (KRCC), to demonstrate how well the generated camera shakiness synchronizes with the actor's emotion. Note here we choose $N = 5$ representative E s $\{0.5, 0.75, 1, 1.5, 2\}$ to depict possible emotional cases for Z_e^h . It can be seen that compared with other models, our method is able to synthesize adaptive shakiness that is highly correlated to the current emotional representation of the actor for achieving a better emotional immersion. Such correlation is further visualized in Fig. 13. In the left of the figure, it is obvious that no matter what the inputted M and C_0 are, the average

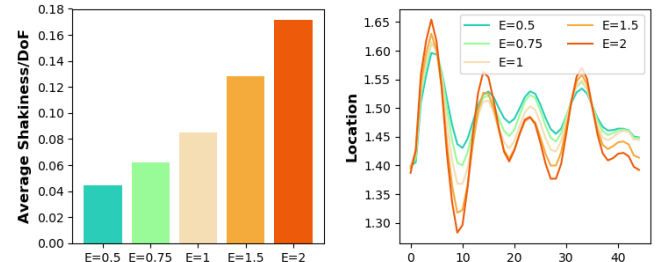


Fig. 13. Detailed verification of the emotional correlation learned by our system. Left: a demonstration of the change of camera shakiness followed by the given character emotion. Right: an example of generated camera trajectory on a certain DoF to show the adaptive shakiness.

shakiness generated for the relaxed emotion ($E < 1$) is suppressed compared to the neutral case ($E = 1$). On the contrary, our camera shakes more distinctly when the intense emotion ($E > 1$) aroused, which is also consistent with the real-world usage of shaky camera. We also illustrate an example of the generated camera trajectories over different E s in the right of Fig. 13, where it can be observe that the learned shakiness adaptation for emotional immersion has little impact on the overall trends of the trajectory for spatial immersion.

4.5.3 Aesthetic immersion. When α and β are both set 0 in Equation (2), frame-level visual aesthetics is mainly counted here for evaluating the sense of immersion. Apart from treating [Yu et al. 2022a], which takes aesthetics into consideration, as a baseline controller model, we also introduce state-of-the-art methods from the image cropping area into the comparison. [Li et al. 2018] and [Hong et al. 2021] are the representatives of novel cropping models, which utilize reinforcement learning and composition-aware Convolutional Neural Networks (CNNs), respectively, to crop images in a way that automates photographic aesthetics. Compared with these methods, it can be verified whether our camera control system Υ enables providing high-level aesthetic frames that satisfy aesthetic immersion.

The two camera control models are tested in 4 3D scenes, where characters differing in age and gender perform 6 untrained actions M in each indoor or outdoor scenery. We obtain C_0 from the initial camera result of [Yu et al. 2022a] while E is randomly picked ranging $(0, 2]$. For each camera controller, 24 cinematic videos are exported and then evenly sampled into 216 frames in total for evaluating the overall visual aesthetics of the corresponding method. The other two image cropping models [Hong et al. 2021; Li et al. 2018] are processed

Table 4. Comparison of aesthetic immersion over image aesthetics score

Model Name	Scene 1 (Library)	Scene 2 (Forest)	Scene 3 (Park)	Scene 4 (Bedroom)	Average
[Yu et al. 2022a]	4.6017	4.8571	4.5665	4.2329	4.5645
[Li et al. 2018]	4.5512	4.8643	4.5070	4.2274	4.5375
[Hong et al. 2021]	4.5645	4.8695	4.5185	4.2498	4.5506
Our System γ	4.8077	5.0970	4.8556	4.4089	4.7923

over the frames of baseline [Yu et al. 2022a] to obtain their results. In order to quantitatively compare the frame-level aesthetics, we leverage a scoring model [Zhao et al. 2020] proposed for Aesthetic Visual Analysis (AVA) tasks, which automatically extracts the hidden aesthetic composition features and predicts scores reflecting the perceptual quality of image aesthetics.

In Table 4, we present the resulting image aesthetics scores for all the tested models. It can be seen that, when applied onto the results of [Yu et al. 2022a], aesthetic improvements brought by cropping models [Hong et al. 2021; Li et al. 2018] are subtle and highly depends on the scenes, while our method enhances frame aesthetics stably regardless of the stage setting. Fig. 14 shows some exampled frames as verification, where we can observe [Yu et al. 2022a] handles basic aesthetic requirements such as character visibility but lacks considering composition. [Li et al. 2018] tries to manage aesthetic composition by inward cropping, however, sometimes such croppings are too aggressive and harm the perceptual quality (see the park case). Another cropping model [Hong et al. 2021] tends to provide limited aesthetic benefits by increasing the saliency of the foreground character. In comparison with these models, our method offers a suitable adjustment to preserve a well-designed composition of each frame for achieving the aesthetic immersion.

Although few works, to the best of our knowledge, addressed metrics assessing cinematographic immersion, the quantitative experiments above have separately manifested the advantages of our method in terms of spatial, emotional, and aesthetic immersion, which can imply that our results are able to satisfy the overall sense of immersion quantitatively. To further confirm this inference, we conduct user studies to evaluate the immersion of our synthesized cinematic videos at the qualitative level.

4.6 Qualitative evaluation of immersion

We perceptually evaluate the immersive performance by conducting a user study to compare our method and the baseline model [Yu et al. 2022a]. Meanwhile, in order to verify the importance of the 3 types of immersion mentioned in Equation (2) that contribute to the overall sense of immersion, we also include variants of our method in the testing for comparison. By disabling parts of the corresponding modules of our method, we can obtain the variant models that focus on different shooting strategies, they are, the model tackling only the spatial immersion (S.I.), the model tackling the spatial and emotional immersion (S.I. + E.I.), as well as the model tackling the spatial and aesthetic immersion (S.I. + A.I.). These 3 variant models, combined with our method (S.I. + E.I. + A.I.) and the

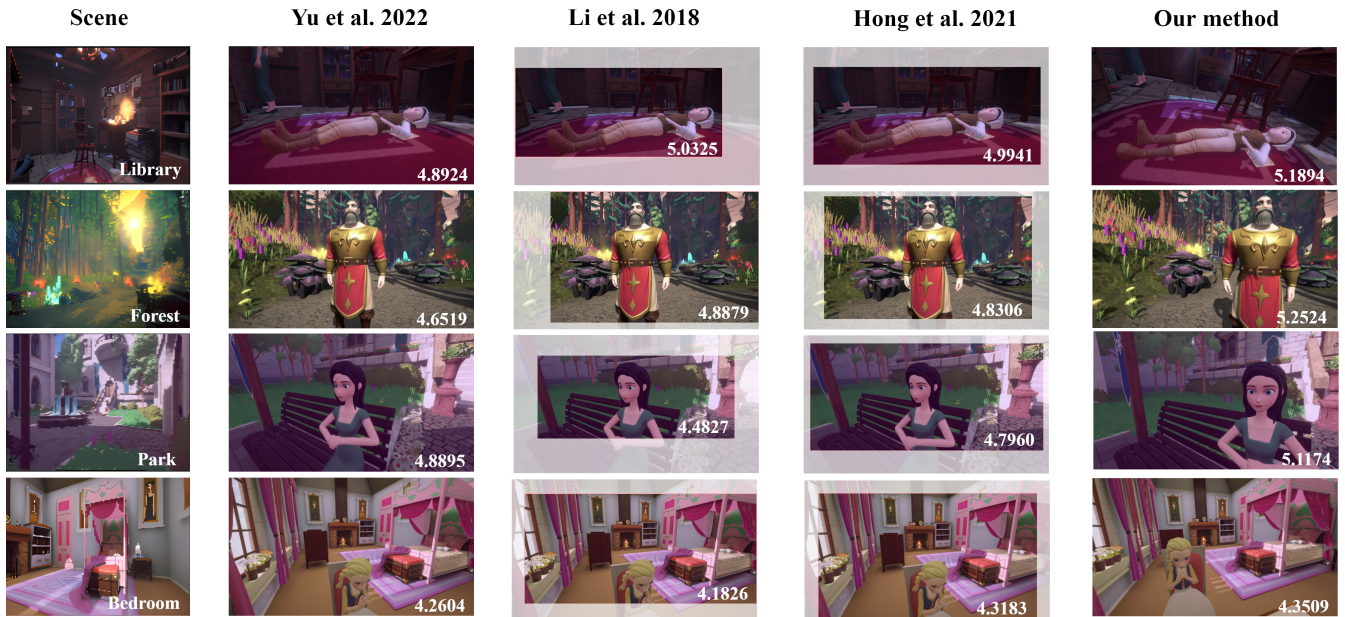


Fig. 14. Examples of aesthetic comparison based on diverse scenes. We demonstrate frames at a certain moment processed by different methods, attaching with aesthetic scores predicted by [Zhao et al. 2020].

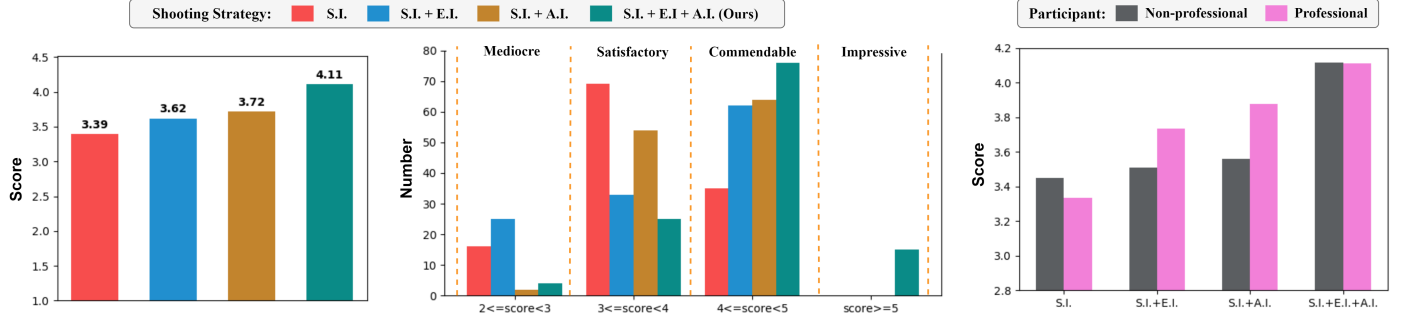


Fig. 15. Rating result of the user study in terms of the immersive enhancement compared to the baseline [Yu et al. 2022a]. Left: average scores of our method and its variants using different shooting strategies. Middle: histogram of score distributions over the 4 tested methods. Right: comparison of scores between professional and non-professional participants.

baseline model [Yu et al. 2022a], are used for qualitatively evaluating the sense of immersion.

Twelve people are invited to the test. Half of them have cinematography related background knowledge while the other half are not. Participants are shown 10 groups of testing videos during the user study. In each group, they are given a short paragraph of scripts that describes the story plot and current scenario, containing the main character, his or her action, and mental status. With the awareness of the scripts, participants first watch the video generated using the baseline model [Yu et al. 2022a] and then 4 other videos using the variant models and our method. They are asked to rate scores for our method and the variant models based on how much the enhancement of immersion they observe compared to the performance of the baseline model [Yu et al. 2022a]. The ratings are from 1 to 5 on a scale of 0.5, where the higher the value of the score, the more enhanced immersion is thought to be brought by the method in comparison with the baseline [Yu et al. 2022a]. More details of user study can be found in Appendix C.

Fig. 15 demonstrates the results of the qualitative evaluation. In the left part of Fig. 15, we can observe that in comparison with the baseline model [Yu et al. 2022a], both of our method and its variants obtain average scores over 3, which means they are thought capable of providing improved immersive performance. From the perspective of shooting strategy, every time an additional type of immersion is considered in the method, accordingly a higher score can be achieved for perceptually enhancing the immersion. Particularly, our method, which can simultaneously handle spatial, emotional, and aesthetic immersion, outperforms the other variant models with a relatively better score.

In the middle part of Fig. 15, we illustrate the detailed score distribution over models using different shooting strategies. It can be observed that, when introducing the strategy tackling the emotional immersion (E.I.), the improved immersive performance of the model S.I. + E.I. is not stable in comparison with that of only considering the spatial immersion (S.I.), by increasing the numbers of “Mediocre” and “Commendable” at the same time. In contrast, the model S.I. + A.I. obtains the immersive enhancement more stably with the additional consideration of the aesthetic immersion (A.I.) upon the model S.I.. Since the model S.I. + E.I. tends to create camera shakiness

for expressing the mental status of the character, the synthesized distinct shakiness can temporally lead to the character being out of the frame in order to cooperate with the performed emotion of high intensity, which partially explains the cases of lower ratings (example can be seen in the Scenario A of Fig. 16). Some other complaints arise from personal preferences that the presented shaking styles are not perfectly fit their expectation. In regard to the good performance of the model S.I. + A.I., the handling of the aesthetic immersion is based on empirical rules suggesting shot angles concluded referring to practical feedback of viewer experience, which accordingly favors the participants during the user study. Hence, taking advantage of shot angles processed for aesthetic immersion, our method that handles all three types of immersion (S.I. + E.I. + A.I.) can alleviate the out-of-frame problem in the variant model S.I. + E.I. and provides high-level performance of immersion. It is also the only model that obtains ratings of the highest level “Impressive”.

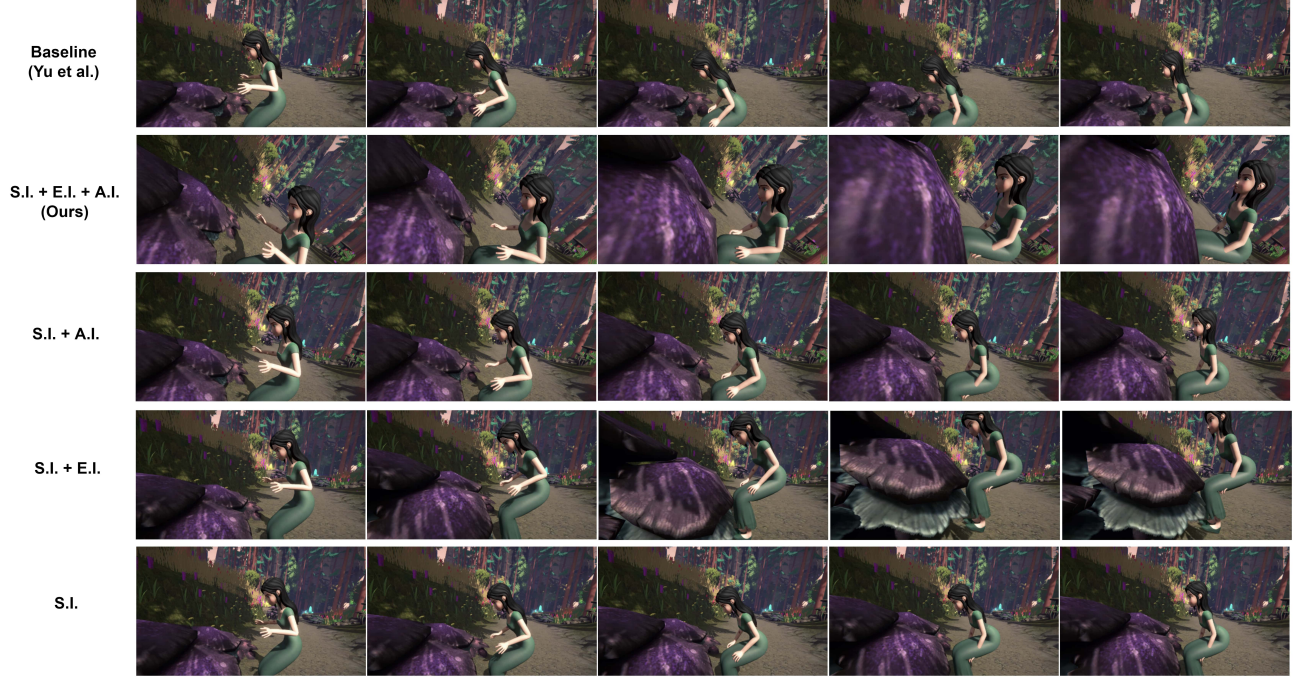
We compare the difference between average scores from professional and non-professional participants for our method and the variant models in the right part of Fig. 15. It can be seen that the non-professional testers are relatively insensitive to the changes of shooting strategy in different models, while the professional testers are more capable of identifying methods that are able to tackle additional types of immersion. Generally, both the professional and non-professional testers agree on the highest immersive enhancement of our model performing the strategy of all three types of immersion (S.I. + E.I. + A.I.).

Though the results of the user study can be affected by a number of factors, such as cinematographic knowledge, the sensitivity of perception, and individual preference, finally our method can be proven to automatically generate high-quality immersive cinematic videos that meet the requirements of the scenario. Meanwhile, the qualitative evaluation also verifies the validity of Equation (2) that the spatial, emotional, and aesthetic immersion are all contributive in regard to the overall sense of immersion.

We present two examples of the qualitative evaluation in Fig. 16. Compared to the baseline [Yu et al. 2022a], the model S.I. enables the synchronization between the character’s action and camera movement. Improving on this case, the model S.I. + E.I. and S.I. + A.I. further consider the emotion-conditioned moving behavior and

Scenario A

Witch Morgana is betrayed by the prince. Morgana sneaks into the royal garden and casts spells to poison the flowers with great hate. She mutters " Poison! Poison! Come to be poisonous!"



Scenario B

Ethan lost his son in the defending war so now he refuses to take the medal of honor heartbrokenly. He shouts to the messenger " Take it away! I hate the golden medal! "



Fig. 16. Two examples of qualitative comparison of cinematographic immersion. Frames obtained from different methods are shown in temporal order from left to right.

aesthetic frame compositions during camera control, respectively. Finally, our method combines all the shooting improvements of the variant models above in order to create an optimal sense of immersion. Live samples can be seen in the supplementary video.

5 DISCUSSION AND CONCLUSION

In this work, we have designed a camera control system that can automatically generate actor-driven camera movements in a 3D virtual environment. Our system is intended to help individuals and corporations create immersive cinematic videos more conveniently. Although the sense of immersion in real-world cinematography is created in various ways according to the director's style and preference, we have analyzed the spatial, emotional, and aesthetic specifications that contribute to the overall cinematographic immersion. These specific components are subsequently combined into a high-level evaluation mechanism that measures the immersive performance of a cinematic sequence. To cooperate with this mechanism, we propose a GAN-based framework to synthesize actor-driven camera trajectories that produce filmic videos with spatial, emotional, and aesthetic immersion.

The proposed encoder-decoder architecture in the generation flow is designed to transfer character actions and emotions from character-space to camera-space behaviors. This allows us to mimic cinematographic techniques such as tracking and shaky camera, which contribute to spatial and emotional immersion for the viewer, respectively, by achieving physical and psychological synchronization between the character and camera. We also incorporate a regularizer that controls the learned camera shakiness, thereby strengthening emotional expression. To achieve aesthetic immersion, we pursue aesthetic frame compositions using a self-supervised adjustment network that follows the rule-of-thirds. In this way, we can adjust the generated camera placements based on analyzing the aesthetic on-frame location of the character via projection.

We have demonstrated the immersive performance of our method through both quantitative and qualitative experiments. Our camera control system has outperformed its variants and a state-of-the-art model. Furthermore, the qualitative evaluation has shown that all three types of immersion - spatial, emotional, and aesthetic - are contributive to perceptual immersion.

It is important to note that various shooting techniques can be used to tackle specific types of immersion. Based on our proposed evaluation mechanism and generation flow, the presentation of synthesized immersive videos is not limited to the three techniques used in our method. A future direction is to extend the pool of immersive shooting techniques under the existing framework so that the control system can offer a wider style of camera behaviors, resulting in a more diverse immersive experience.

APPENDIX

A CINEMATOGRAPHIC TECHNIQUES

Tracking camera: A typical technique focusing on spatial immersion, which considers that the camera should move following the motion of the actor carefully [Brown 2016], including fine-grained action in place (e.g. stand, sit) or general transition between the place (e.g. run, walk). We demonstrate an example from *Mindhunter* in Fig.

1(a). Comparing the backgrounds shown in time-sequence frames, it can be seen that camera tilt is applied in the shooting to follow the raising of the actor's head, which provides an observational style that actively enhances the experience of the audience.

Shaky camera: A popular technique for emotional immersion, which leverages intentional unsteadiness [Mekas 1962] to express the psychological status of the actor. More specifically, the ways to present camera shakiness (i.e. the control of amplitude and frequency) should be consistent with the category and intensity of the emotion performed by the actor [Morgan 2013]. In Fig. 1(b), we sample the footage from *Succession*, where the actor is shouting in front of the camera angrily. Accordingly, camera provides a large amplitude of shakiness (see the change of drawings in the background) to make audiences feel the anger of the actor and arouse their tension.

Rule-of-thirds: It is one of the most famous principles [Wright 2017] to control frame composition for aesthetic immersion. The rule requires that the actor's body should be placed at a specific one-third part of the shot [Krages 2012] considering factors like, actor pose and leading room [May 2020], to earn the audience's attraction and affection. As an example 1(c) obtained from *Mission Impossible - Fallout*, no matter how the camera moves, it carefully keeps the on-frame location of the actor's body staying on the left one-third alignment line to provide aesthetic pleasure for the audience.

More live examples of masterpieces utilizing the three shooting techniques can be watched in the supplementary video.

B IMPLEMENTATION OF AESTHETIC LOSS

In this section we introduce implementation details regarding camera projection, decision tree, and derivation process of the utilized variables.

Camera projection: We denote the process of camera projection as f_p to simplify the explanation. Given an arbitrary pair of actor joint $P_j \in \mathbb{R}^Q$ and \tilde{C}_0 , we can obtain the projection result $P_{2d} \in \mathbb{R}^2$ by performing $f_p(P_j, \tilde{C}_0)$ so as to localize the actor joint from 3D world to 2D shot.

The first step handles the transformation between world coordinate P_w and camera coordinate P_c . Since $P_w = [X_w, Y_w, Z_w, 1]^T$ can be constructed using the position of P_j , we can derive $P_c = [X_c, Y_c, Z_c, 1]^T$ by:

$$P_c = R_c T_c P_w, \quad (19)$$

where R_c and T_c are 4×4 rotation and translation matrix created based on the corresponding location of \tilde{C}_0 , respectively.

In the second step, we need to transform P_c into the sensor coordinate $P_i = [x, y, 1]^T$ (i.e. the image plane inside the camera) by:

$$P_i = V_p P_c, \quad (20)$$

where V_p is a 3×4 perspective projection matrix built with the focal length of the camera and Z_c .

Finally, to localize P_j on the shot, P_i should be scaled and translated to the shot coordinate $P_s = [u, v, 1]^T$ referring to camera intrinsics, which can be formed as:

$$P_s = T_s P_i, \quad (21)$$

where T_s denotes a 3×3 transformation matrix handling the scaling and translation performed on x and y axis.

The 2D joint projection P_{2d} can then take the form of (u, v) obtained from values in P_s . Similarly, when projecting the whole actor pose, f_p follows the same process above by applying multi-dimensional matrix operations.

Projection-related variables: Based on the camera projection process f_p , related variables that utilized in the loss components can be derived as follows:

- M_{2d} is obtained by $f_p(M_0, \hat{C}_0 + C_0 \Delta)$. Based on the actual size of shot, joints detected off-frame are set $(0, 0)$.
- \bar{M}_{2d} is obtained by calculating the weighted mean of M_{2d} , where the weights follow normal distribution. The torso joints are weighted as the peak of the distribution, while weights of the other joints get decreased based on how far the joints are away from the torso. Note here we exclude off-frame joints in the operation.
- M_b is obtained from binarizing M_{2d} in order to show whether the specific joint is on-frame (labeled as 1) or off-frame (labeled as 0). Since M_{2d} are non-negative, we add up the projected u and v coordinate of each joint and set 0 as threshold when performing binarization.
- M'_b is obtained following the same process of M_b . Instead of using the adjusted camera placement, its derivation is based on the original camera placement \hat{C}_0 .

Decision tree an alignment: Our decision tree is used for deriving candidates of alignment A_l that determines the performance of aesthetic composition. Following the strategy in Fig. 6, the factor actor pose is represented by height difference hpd between head and pelvis, while shot side is defined by relative angle ra between camera and actor. Assume \bar{M}_{2d} is obtained as (u_m, v_m) and each shot is in the size of $(width, height)$, $A_l = \{(u_1, v_1), (u_2, v_2)\}$ can be derived as follow:

C PROCESS OF USER STUDY

In this section, we clarify some additional details for the process of the user study as a supplement to Section 4.6. The main flow can be seen in Fig. 17. Before the test, all the participants are briefly introduced to the 3 types of immersion in terms of spatial, emotional, and aesthetic level, along with the corresponding shooting techniques of tracking camera, shaky camera, and rule-of-thirds, to benefit the understanding of the testing contents. At the beginning of the test, we ask participants whether they have experience or background knowledge of cinematography, so as to mark them as professional or non-professional testers. Then, When entering each test group, the participants are shown scripts of the scenario, where the important descriptions are highlighted with distinct colors. Being aware of the scripts, the participants are first shown a video generated by baseline [Yu et al. 2022a], which is named V000. Then, they need to watch another 4 videos generated using our method and the variants models. These 4 videos are randomly named from V001 to V004 in order to avoid the conventional thinking of the participants in the

ALGORITHM 1: Deriving Alignment Candidates

```

{(u1, v1), (u2, v2)} ← {(0, 0), (0, 0)};
thres ← Lie-to-stand threshold;
if hpd ≥ thres then // Confirmed stand pose
    if ra ∈ [45°, 135°] then // Confirmed right shot
        u1, u2 ← 1/3 width;
        v1, v2 ← vm;
    else if ra ∈ [225°, 315°] then // Confirmed left shot
        u1, u2 ← 2/3 width;
        v1, v2 ← vm;
    else // Confirmed front or back shot
        u1 ← 1/3 width;
        u2 ← 2/3 width;
        v1, v2 ← vm;
    end
else
    if ra ∈ [45°, 135°] ∪ [225°, 315°] then
        v1 ← 1/3 height;
        v2 ← 2/3 height;
        u1, u2 ← um;
    else
        u1 ← 1/3 width;
        u2 ← 2/3 width;
        v1, v2 ← vm;
    end
end

```

testing. For convenience, we provide side-by-side videos comparing the baseline V000 and videos based on the other methods to benefit human perception. After watching all the videos, the participants are required to rate the immersive enhancement of the videos from V001 to V004 in comparison with V000. Referring to the description of the rating choice, scores less than 3 denote that this method is not capable to offer an improved immersion compared with the baseline [Yu et al. 2022a], while scores over 3 confirm the improvement in the immersive performance of the method. Finally, all the submitted test results are collected together for the subsequent data analysis.

REFERENCES

Hadi AlZayer, Hubert Lin, and Kavita Bala. 2021. AutoPhoto: Aesthetic Photo Capture using Reinforcement Learning. In *2021 IEEE/RSJ International Conference on Intelligent Robots and Systems (IROS)*. IEEE, 944–951.

Ido Arev, Hyun Soo Park, Yaser Sheikh, Jessica Hodgins, and Ariel Shamir. 2014. Automatic editing of footage from multiple social cameras. *ACM Transactions on Graphics (TOG)* 33, 4 (2014), 1–11.

Rudolf Arnheim. 1956. *Art and visual perception: A psychology of the creative eye*. Univ of California Press.

Nikunj Arora, Markku Suomalainen, Matti Pouke, Evan G Center, Katherine J Mimnaugh, Alexis P Chambers, Sakaria Pouke, and Steven M LaValle. 2022. Augmenting immersive telepresence experience with a virtual body. *arXiv preprint arXiv:2202.00900* (2022).

Staffan Björk and Jussi Holopainen. 2005. Games and design patterns. *The game design reader: A rules of play anthology* (2005), 410–437.

Rogerio Bonatti, Arthur Bucker, Sebastian Scherer, Mustafa Mukadam, and Jessica Hodgins. 2021. Batteries, camera, action! learning a semantic control space for expressive robot cinematography. In *2021 IEEE International Conference on Robotics and Automation (ICRA)*. IEEE, 7302–7308.

Rogerio Bonatti, Wenshan Wang, Cherie Ho, Aayush Ahuja, Mirko Gschwindt, Efe Camci, Erdal Kayacan, Sanjiban Choudhury, and Sebastian Scherer. 2020. Autonomous aerial cinematography in unstructured environments with learned artistic decision-making. *Journal of Field Robotics* 37, 4 (2020), 606–641.



Fig. 17. Main testing flow for the user study. See the texts above for details.

Blain Brown. 2016. *Cinematography Theory and Practice: Imagemaking for Cinematographers & Directors*. Routledge.

Paolo Burelli. 2016. Game Cinematography: From Camera Control to Player Emotions. In *Emotion in Games*. Springer, 181–195.

Sumit Chopra, Raia Hadsell, and Yann LeCun. 2005. Learning a similarity metric discriminatively, with application to face verification. In *2005 IEEE Computer Society Conference on Computer Vision and Pattern Recognition (CVPR'05)*, Vol. 1. IEEE, 539–546.

Xiangtong Chu, Xiao Xie, Shuainan Ye, Haolin Lu, Hongguang Xiao, Zeqing Yuan, Zhiutian Chen, Hui Zhang, and Yingcai Wu. 2021. TIVEE: Visual exploration and explanation of badminton tactics in immersive visualizations. *IEEE Transactions on Visualization and Computer Graphics* 28, 1 (2021), 118–128.

Junyoung Chung, Caglar Gulcehre, KyungHyun Cho, and Yoshua Bengio. 2014. Empirical evaluation of gated recurrent neural networks on sequence modeling. *arXiv preprint arXiv:1412.3555* (2014).

Yuanjie Dang, Chong Huang, Peng Chen, Ronghua Liang, Xin Yang, and Kwang-Ting Cheng. 2020. Imitation learning-based algorithm for drone cinematography system. *IEEE Transactions on Cognitive and Developmental Systems* 14, 2 (2020), 403–413.

Yuanjie Dang, Chong Huang, Peng Chen, Ronghua Liang, Xin Yang, and Kwang-Ting Cheng. 2022. Path-Analysis-Based Reinforcement Learning Algorithm for Imitation Filming. *IEEE Transactions on Multimedia* (2022).

Thomas Flight. 2021. *The Succession Character You Never See*. https://www.youtube.com/watch?v=_IU91279xZk

Quentin Galvane. 2015. *Automatic Cinematography and Editing in Virtual Environments*. Ph.D. Dissertation. Université Grenoble Alpes (ComUE).

Mirko Gschwindt, Efe Camci, Rogerio Bonatti, Wenshan Wang, Erdal Kayacan, and Sebastian Scherer. 2019. Can a robot become a movie director? learning artistic principles for aerial cinematography. In *2019 IEEE/RSJ International Conference on Intelligent Robots and Systems (IROS)*. IEEE, 1107–1114.

Philippe Guillotet, Fabien Danieau, Julien Fleureau, Ines Rouxel, and M Christie. 2016. Introducing Basic Principles of Haptic Cinematography and Editing.. In *WICED@ Eurographics*. 15–21.

Kyle De Guzman. 2021. *The Arc Shot – Examples and Camera Movements Explained*. <https://www.studiobinder.com/blog/arc-shot-in-film-definition/>

Masaki Hayashi, Seiki Inoue, Mamoru Douke, Narichika Hamaguchi, Hiroyuki Kaneko, Steven Bachelder, and Masayuki Nakajima. 2014. T2V: New Technology of Converting Text to CG Animation. *ITE Transactions on Media Technology and Applications* 2, 1 (2014), 74–81.

Martin Heusel, Hubert Ramsauer, Thomas Unterthiner, Bernhard Nessler, and Sepp Hochreiter. 2017. Gans trained by a two time-scale update rule converge to a local nash equilibrium. *Advances in neural information processing systems* 30 (2017).

Chaoyi Hong, Shuaiyuan Du, Ke Xian, Hao Lu, Zhiguo Cao, and Weicai Zhong. 2021. Composing photos like a photographer. In *Proceedings of the IEEE/CVF Conference on Computer Vision and Pattern Recognition*. 7057–7066.

Chong Huang, Yuanjie Dang, Peng Chen, Xin Yang, and Kwang-Ting Cheng. 2021. One-shot imitation drone filming of human motion videos. *IEEE Transactions on Pattern Analysis and Machine Intelligence* 44, 9 (2021), 5335–5348.

Chong Huang, Chuan-En Lin, Zhenyu Yang, Yan Kong, Peng Chen, Xin Yang, and Kwang-Ting Cheng. 2019. Learning to film from professional human motion videos. In *Proceedings of the IEEE/CVF Conference on Computer Vision and Pattern Recognition*. 4244–4253.

Matt Jacobs. 2018. *What Is a Zoom Shot? Definition and Examples*. <https://filmlifestyle.com/zoom-shot/>

Hongda Jiang, Marc Christie, Xi Wang, Libin Liu, Bin Wang, and Baoquan Chen. 2021. Camera keyframing with style and control. *ACM Transactions on Graphics (TOG)* 40, 6 (2021), 1–13.

Hongda Jiang, Bin Wang, Xi Wang, Marc Christie, and Baoquan Chen. 2020. Example-driven virtual cinematography by learning camera behaviors. *ACM Transactions on Graphics (TOG)* 39, 4 (2020), 45–1.

Sarah Jones and Steve Dawkins. 2018. Walking in someone else's shoes: Creating empathy in the practice of immersive film. *Media Practice and Education* 19, 3 (2018), 298–312.

Iason Karakostas, Ioannis Mademlis, Nikos Nikolaidis, and Ioannis Pitas. 2020. Shot type constraints in UAV cinematography for autonomous target tracking. *Information Sciences* 506 (2020), 273–294.

Shunichi Kasahara, Shohei Nagai, and Jun Rekimoto. 2016. Jackin head: Immersive visual telepresence system with omnidirectional wearable camera. *IEEE transactions on visualization and computer graphics* 23, 3 (2016), 1222–1234.

Sangwook Kim, Kyungae Cha, Mansoo Kim, and Eetaek Lee. 1998. 3D Animation using Visual Script Language. In *The Fifth International Workshop on Distributed Multimedia Systems, Taiwan*. Citeseer, 109–113.

Diederik P Kingma and Jimmy Ba. 2014. Adam: A method for stochastic optimization. *arXiv preprint arXiv:1412.6980* (2014).

Bert Krages. 2012. *Photography: the art of composition*. Simon and Schuster.

S.C. Lannom. 2019. *Eye Level Shots: Creative Examples of Camera Angles and Shots*. <https://www.studiobinder.com/blog/eye-level-camera-shot-angle/>

Mackenzie Leake, Abe Davis, Anh Truong, and Maneesh Agrawala. 2017. Computational video editing for dialogue-driven scenes. *ACM Trans. Graph.* 36, 4 (2017), 130–1.

Hsin-Ying Lee, Xiaodong Yang, Ming-Yu Liu, Ting-Chun Wang, Yu-Ding Lu, Ming-Hsuan Yang, and Jan Kautz. 2019. Dancing to music. *Advances in neural information processing systems* 32 (2019).

Debang Li, Huikai Wu, Junge Zhang, and Kaiqi Huang. 2018. A2-RL: Aesthetics aware reinforcement learning for image cropping. In *Proceedings of the IEEE conference on computer vision and pattern recognition*. 8193–8201.

Chao Liang, Changsheng Xu, Jian Cheng, WeiQing Min, and Hanqing Lu. 2012. Script-to-movie: a computational framework for story movie composition. *IEEE transactions on multimedia* 15, 2 (2012), 401–414.

Amaury Louarn, Marc Christie, and Fabrice Lamarche. 2018. Automated staging for virtual cinematography. In *Proceedings of the 11th Annual International Conference on Motion, Interaction, and Games*. 1–10.

Harri Mäcklin et al. 2019. Going Elsewhere: A Phenomenology of Aesthetic Immersion. (2019).

Aravindh Mahendran and Andrea Vedaldi. 2015. Understanding deep image representations by inverting them. In *Proceedings of the IEEE conference on computer vision and pattern recognition*. 5188–5196.

Christopher D Manning. 2009. *An introduction to information retrieval*. Cambridge university press.

Pete May. 2020. *Essential Digital Video Handbook: A Comprehensive Guide to Making Videos That Make Money*. Routledge.

Jonas Mekas. 1962. A Note on the Shaky Camera. *Film Culture* 24–27 (1962), 40.

Morgan. 2013. *Camera Movement Tutorial: How To Create Emotion*. <https://theslantedlens.com/2013/camera-movement-tutorial-how-to-create-emotion/>

Nicholas T Proferes. 2005. *Film Directing Fundamentals: see your film before shooting*. Taylor & Francis.

Pablo Pueyo, Eduardo Montijano, Ana C Murillo, and Mac Schwager. 2022. CineMPC: Controlling Camera Intrinsic and Extrinsic for Autonomous Cinematography. In *2022 International Conference on Robotics and Automation (ICRA)*. IEEE, 4058–4064.

Evan Puschak. 2017. How David Fincher Hijacks Your Eyes. <https://www.youtube.com/watch?v=GfqD5WqChUY>

Frank Rose. 2012. *The art of immersion: How the digital generation is remaking Hollywood, Madison Avenue, and the way we tell stories*. WW Norton & Company.

Mohamed Sayed, Robert Cinca, Enrico Costanza, and Gabriel Brostow. 2022. Lookout! interactive camera gimbal controller for filming long takes. *ACM Transactions on Graphics (TOG)* 41, 3 (2022), 1–16.

Karen Simonyan and Andrew Zisserman. 2014. Very deep convolutional networks for large-scale image recognition. *arXiv preprint arXiv:1409.1556* (2014).

Richard Skarbez, Frederick P Brooks, and Mary C Whitton. 2020. Immersion and coherence: Research agenda and early results. *IEEE transactions on visualization and computer graphics* 27, 10 (2020), 3839–3850.

Hariharan Subramonyam, Wilmot Li, Eytan Adar, and Mira Dontcheva. 2018. Take-toons: Script-driven performance animation. In *Proceedings of the 31st Annual ACM Symposium on User Interface Software and Technology*. 663–674.

Yaniv Taigman, Ming Yang, Marc'Aurelio Ranzato, and Lior Wolf. 2014. Deepface: Closing the gap to human-level performance in face verification. In *Proceedings of the IEEE conference on computer vision and pattern recognition*. 1701–1708.

Anh Truong, Floraine Berthouzoz, Wilmot Li, and Maneesh Agrawala. 2016. Quickcut: An interactive tool for editing narrated video. In *Proceedings of the 29th Annual Symposium on User Interface Software and Technology*. 497–507.

Ashish Vaswani, Noam Shazeer, Niki Parmar, Jakob Uszkoreit, Llion Jones, Aidan N Gomez, Łukasz Kaiser, and Illia Polosukhin. 2017. Attention is all you need. *Advances in neural information processing systems* 30 (2017).

Valentijn T Visch, Ed S Tan, and Dylan Molenaar. 2010. The emotional and cognitive effect of immersion in film viewing. *Cognition and Emotion* 24, 8 (2010), 1439–1445.

Jianyi Wang, Mai Xu, Lai Jiang, and Yuhang Song. 2020. Attention-Based Deep Reinforcement Learning for Virtual Cinematography of 360 degree Videos. *IEEE Transactions on Multimedia* 23 (2020), 3227–3238.

Miao Wang, Guo-Wei Yang, Shi-Min Hu, Shing-Tung Yau, and Ariel Shamir. 2019. Write-a-video: computational video montage from themed text. *ACM Trans. Graph.* 38, 6 (2019), 177–1.

Joseph Williams, Sven Shepstone, and Damian Murphy. 2022. Understanding Immersion in the Context of Films with Spatial Audio. In *Audio Engineering Society Conference: AES 2022 International Audio for Virtual and Augmented Reality Conference*. Audio Engineering Society.

Steve Wright. 2017. *The Rule Of Thirds: What is it? Filmmaking and Photography Training*. <https://www.youtube.com/watch?v=A7wnhDKyBuM>

Hui-Yin Wu, Francesca Palù, Roberto Ranon, and Marc Christie. 2018. Thinking like a director: Film editing patterns for virtual cinematographic storytelling. *ACM Transactions on Multimedia Computing, Communications, and Applications (TOMM)* 14, 4 (2018), 1–22.

Xiaoshan Yang, Tianzhu Zhang, and Changsheng Xu. 2018. Text2video: An end-to-end learning framework for expressing text with videos. *IEEE Transactions on Multimedia* 20, 9 (2018), 2360–2370.

Zixiao Yu, Enhao Guo, Haohong Wang, and Jian Ren. 2022a. Bridging Script and Animation Utilizing a New Automatic Cinematography Model. In *2022 IEEE 5th International Conference on Multimedia Information Processing and Retrieval (MIPR)*. IEEE, 268–273.

Zixiao Yu, Chenyu Yu, Haohong Wang, and Jian Ren. 2022b. Enabling Automatic Cinematography with Reinforcement Learning. In *2022 IEEE 5th International Conference on Multimedia Information Processing and Retrieval (MIPR)*. IEEE, 103–108.

Yizhong Zhang, Jiaolong Yang, Zhen Liu, Ruicheng Wang, Guojun Chen, Xin Tong, and Baining Guo. 2022. Virtualcube: An immersive 3d video communication system. *IEEE Transactions on Visualization and Computer Graphics* 28, 5 (2022), 2146–2156.

Lin Zhao, Meimei Shang, Fei Gao, Rongsheng Li, Fei Huang, and Jun Yu. 2020. Representation learning of image composition for aesthetic prediction. *Computer Vision and Image Understanding* 199 (2020), 103024.